Scientific Report No. 99

MODELING SEMI-ANECHOIC ELECTROMAGNETIC MEASUREMENT CHAMBERS

by
Christopher L. Holloway and Edward F. Kuester

Electromagnetics Laboratory
Department of Electrical and Computer Engineering
Campus Box 425
University of Colorado
Boulder, Colorado 80309-0425

August 8, 1990

Prepared for
IBM Corporation

This research was supported by the International Business Machines Corporation, Boulder, Colorado, under a Research Agreement with the University of Colorado at Boulder. The encouragement and technical assistance of Mr. Robert F. German of IBM is gratefully acknowledged.

Abstract

In previous work, we have developed a model to predict theoretically the low-frequency plane-wave reflection coefficient of an array of pyramid cone absorbers such as are used to line anechoic electromagnetic measurement chambers. In this report, we will use this model together with a geometrical-optics approach as building blocks to predict the electromagnetic field in a chamber lined with cone absorbers in the frequency range of 30-300 MHz. The results are compared with site attenuation measurements from two semi-anechoic rooms.

1 Introduction

The Federal Communication Commission (FCC) regulates the amount of electromagnetic radiation electronic equipment can produce over the frequency range of 30 to 1000 MHz. Such equipment must thus be tested to insure compliance with FCC specifications, which require the tests to be made on a so-called "open-field test site"—an outdoor area provided with a ground screen and free from obstacles and interfering ambient fields. Using the open field as a test environment can be inconvenient or even impossible. The tests may not be repeatable due to changing factors in the environment itself (changes in weather conditions can make the conductivity of the earth vary from one day to the next, or interrupt test scheduling). In addition, large amounts of flat land free from buildings and trees required for such a site may not be easily available.

Alternatively, the tests could be made inside a semi-anechoic measurement chamber if the chamber can be shown to correlate well enough with an ideal open field site. This correlation is generally quite good at frequencies higher then 300 MHz, but at lower frequencies (30-300 MHz), large discrepancies are often observed, due to reflections from the chamber walls.

In the previous work [1], it was shown that it is possible to accurately predict the low-frequency plane-wave reflection coefficient of the pyramid cone absorbers used to line the anechoic chambers, and hence to use computer simulation to produce cone designs that have lower reflection than standard absorbing cones in the low-frequency range. This should make it possible to improve the performance of measurement chambers, but to ensure that the desired performance is acheived before the chamber is built, a reliable model is needed to predict the chamber response.

Many papers about the modeling and analysis of anechoic chambers, both electromagnetic and acoustic, appear scattered throughout the literature [2]–[22]. Kolar [2] and later Benham [10] used a physical optics technique to predict the chamber response, and Wright and White [3] used a cavity-mode representation for the chamber field distribution. However, the most popular technique seems to be that of geometrical optics, where a ray representation is used to account for reflections from the absorbing walls, with the assumption that if

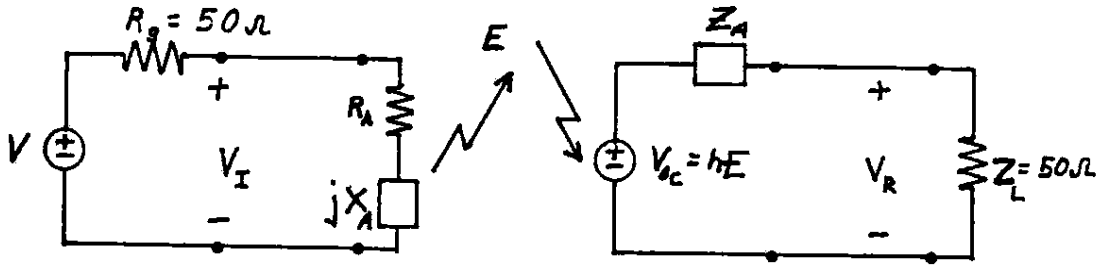

Figure 1: Antenna equivalent circuits: $Z_A = R_A + jX_A$ is the antenna impedance, V_R the received voltage, V_{oc} the open-circuit voltage induced by the electric field E, and h the effective height of the antenna.

a wave makes more than one bounce off an absorbing surface it is negligible. A refinement of this technique has been made that takes into account multiple reflections of the waves [17], [22]. The ray method has also been used to analyze chambers of shape other than rectangular [5]-[11], [15], [18]-[20].

The single-bounce ray method will be used here to develop a theoretical model to predict chamber performance. In contrast to the earlier uses of this method, we make use of the results of [1] to provide accurate information on the amplitude and phase of the wall reflection coefficients. We should thus expect much better agreement with measured results in actual chambers. The response of these chambers is measured by a quantity known as site attenuation [23]–[27], and the model presented here will be used to predict this quantity.

2 Site Attenuation

The site attenuation for any measurement site is defined in terms of equivalent circuits for the transmitting and receiving antennas (Figure 1) [26]:

$$A = \frac{V_I}{V_R} \tag{1}$$

where V_I is the voltage at the transmitting antenna terminals, and V_R is the voltage at the load impedance connected to the receiving antenna. The site attenuation may be related to the antenna and site properties more directly by making use of a quantity known as the *antenna factor* a_F for both of the antennas in the measurement scheme. The antenna factor a_{FR} of a receiving antenna is defined as the ratio of the magnitude E of the incident electric field component parallel to the antenna axis to the magnitude of the load voltage V_R

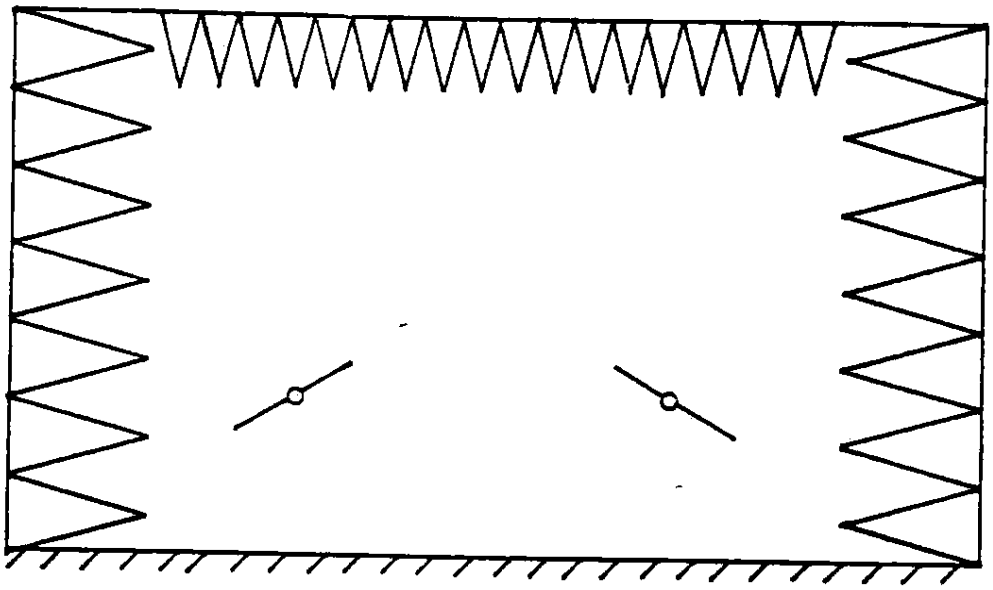

Figure 2: Illustration of chamber.

produced by the antenna across its load:

$$V_R = \frac{E}{a_{FR}} \tag{2}$$

while that of the transmitting antenna is defined analogously, and using reciprocity we can show that the antenna factors of the same antenna are identical for the transmitting and receiving cases. The antenna factor can be related to the *effective height* h of the antenna, which is defined as the ratio of the magnitude of the open-circuit voltage V_{oc} induced at the antenna terminals to the incident field E defined above:

$$h = \frac{V_{oc}}{E}$$

In the simple equivalent circuit shown in Figure 1, the receiving antenna has an antenna factor of $(Z_A + Z_{\text{load}})/Z_{\text{load}}h$. In practice, however, effects of baluns, cables, attenuators and so forth make this relation more complicated. In any case, a_F can be determined from calibration measurements at any given test site [26].

If the generator is matched to the transmitting antenna, the open-circuit voltage V of the signal generator will be twice the output voltage V_I:

$$V = 2V_I \tag{3}$$

The chamber to be modeled in this study is semi-anechoic (the floor is virtually an ideal conductor while the walls and ceiling are lined with absorbing material) and contains transmitting and receiving antennas placed along the centerline of the room (Figure 2). The field strength E along the axis of the receiving antenna can be given in terms of the open-circuit generator voltage V, the transmitting

antenna factor a_{FT} and the paths taken by various waves incident directly or after reflection at the receiving antenna:

$$E = \frac{V f_m}{79.58 a_{FT}} E_{H,V} \tag{4}$$

Here f_m is the frequency in MHz, and $E_{H,V}$ is a normalized electric field at the receiving antenna that depends on the antenna pattern, the reflection coefficients at the walls and the total distances r_n of propagation for each of the constituent waves in the chamber that is incident onto the receiving antenna:

$$E_{H,V} = |\{\sum_{n=1}^{N} [\frac{e^{-jk_0 r_n}}{r_n} \rho_n F_{T_n} F_{R_n}]\}| \tag{5}$$

where k_0 is the wavenumber of free space, N is the total number of rays (that is, the individual paths from the source to the receiver), ρ_n is the reflection coefficient for each ray as it reflects off the walls, and F_{T_n}, F_{R_n} are the antenna pattern factors associated with each ray path at the transmitting and receiving antenna respectively. The subscripts H and V correspond to the polarization of the two antennas inside the chambers (H for horizontal and V for vertical).

Substituting (3)-(4) into (1), the following is obtained:

$$A = \frac{279.1 a_{FR} a_{FT}}{f_m} (\frac{1}{E_{H,V}}) \tag{6}$$

If the receiving and the transmitting antenna factors are equal ($a_{FT} = a_{FR} \equiv a_F$), then (6) expressed in dB becomes:

$$A(dB) = -20\log(f_m) + 48.92 + 2a_F(dB/m) - E_{H,V}(dB\mu V/m) \tag{7}$$

3 Open Field Analysis

If the absorbers on the walls and the ceiling of the chamber performed ideally, there would be only two rays incident upon the receiving antenna; one directly from the transmitting antenna, and one which reflects from the floor. It would then be functionally identical to an ideal open-field site (where the ground is assumed to be a perfect conductor). The site attenuation of the chamber will thus be compared to that of an open-field site in order to get an indication of the quality of the chamber, for both horizontal and vertical polarizations.

An ideal open-field site with the antenna oriented in the horizontal polarization is shown in Figure 3. As illustrated there, r_1 is the distance traveled by the ray directed from the transmitting to the receiving antenna, while r_2 is the distance traveled by the ray that bounces off of the ground (perfect conductor). Therefore, equation (5) becomes:

$$E_H = |\{\frac{e^{-jk_0 r_1}}{r_1} + \frac{e^{-jk_0 r_2}}{r_2} \rho_2\}| \tag{8}$$

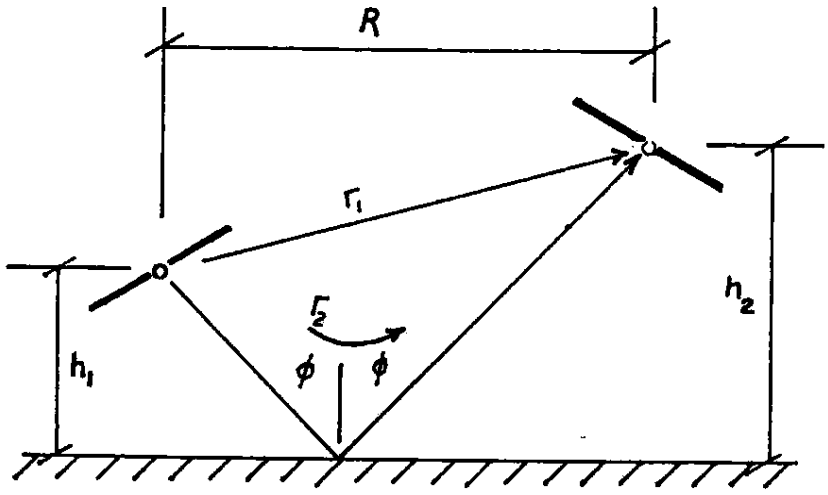

Figure 3: Open-field site

In the cases to be examined in this work, the two antennas are set 3 meters apart horizontally, and are 1.5 meters off the ground for the case of horizontal polarization and 1.0 meter off the ground for vertical polarization. A computer program was written to calculate the site-attenuation for the frequency range 30 to 200 MHz. The results for the horizontal polarization are shown in Figure 4. Note that $\rho_2 = -1$ for this case. Results for the case of vertical polarization are shown in Figure 5 (here $\rho_2 = 1$).

4 Model of the Chamber

In this section a general one-bounce chamber model is developed. Since semi-anechoic chambers have a metal floor, image theory can be utilized in order to assist the analysis. The metal floor is removed and the height of the chamber is doubled. The new floor of the chamber is lined with the same type of absorber that is on the ceiling, and an additional imaged transmitting antenna is placed below the actual transmitting antenna (Figure 6).

For the analysis of the chamber, four assumptions are made:

1. The fields that are incident onto the wall are locally plane waves.

2. Geometrical optics is used to compute the waves reflected from the chamber walls. That is, the angle at which the wave reflects from the wall is taken to be equal to the angle of incidence of the wave.

3. The walls are in the far-field of both the transmitting and receiving antennas.

4. Only waves from the transmitting antenna that have made no more than one bounce from an absorbing wall before becoming incident onto the

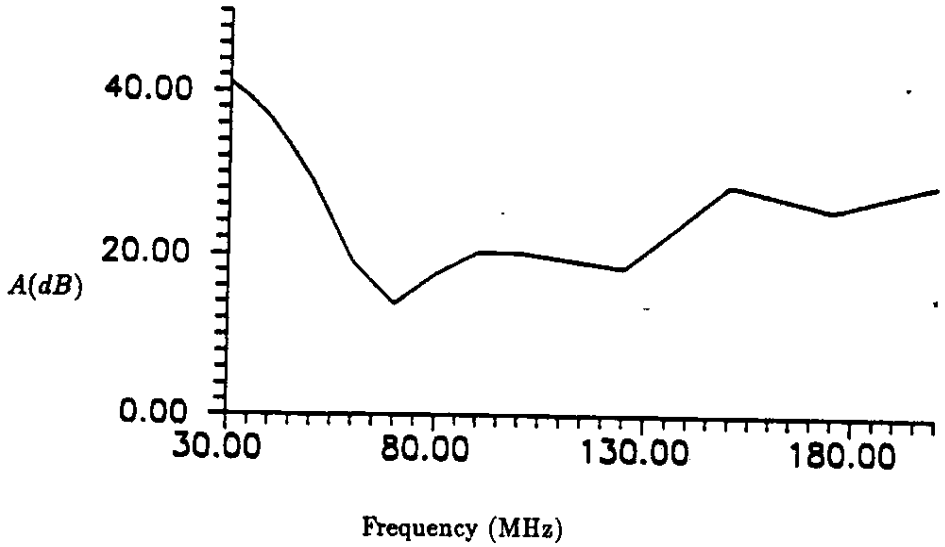

Figure 4: Theoretical open-field site attenuation for horizontal polarization.

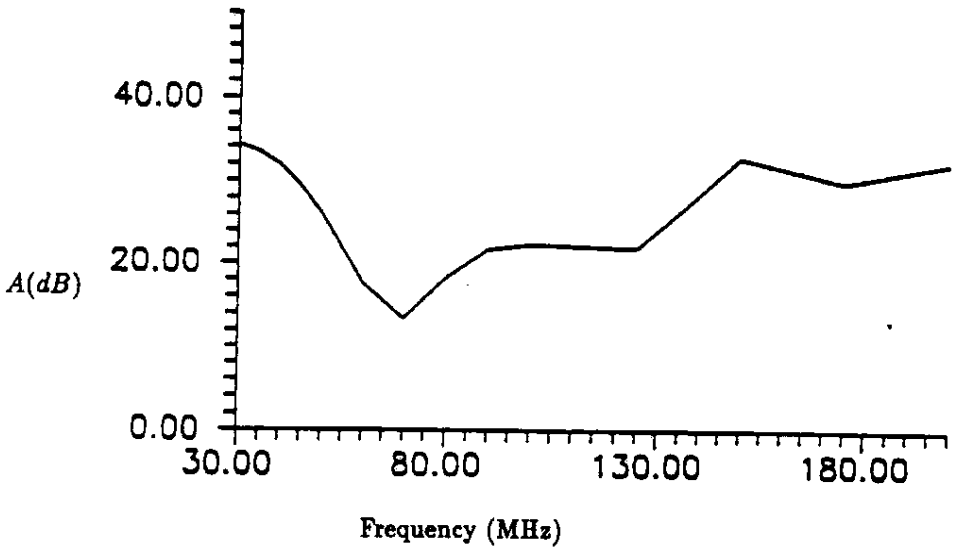

Figure 5: Theoretical open-field site attenuation for vertical polarization.

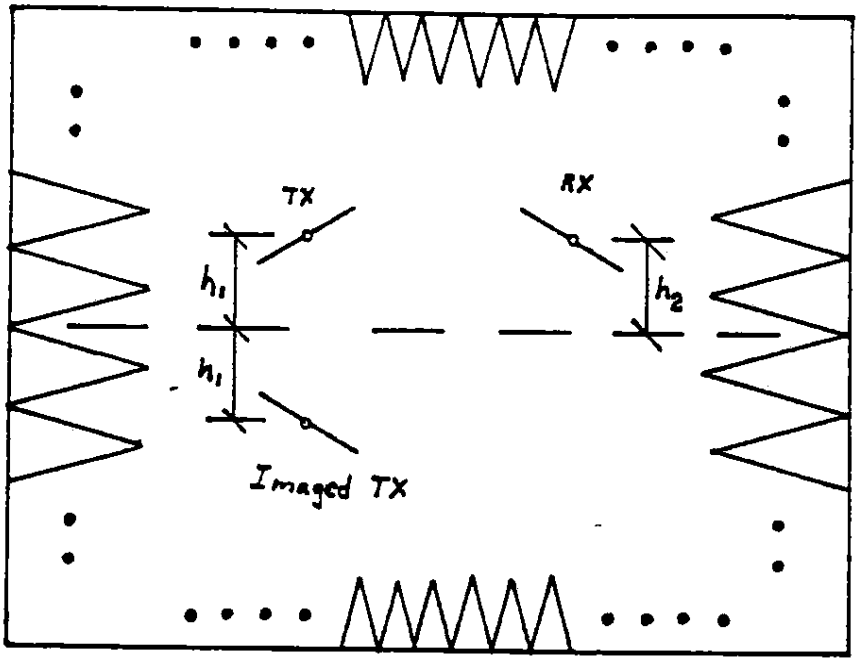

Figure 6: Imaged antenna and chamber configuration.

receiving antenna are considered. It is assumed that if the wave makes two bounces from an absorbing surface, the magnitude of the wave is negligible.

From assumptions 2 and 4, we find that only fourteen individual rays need to be considered. Starting from the transmitting antenna there are: 1) one ray that is directed straight to the receiving antenna, 2) one ray off each side wall, 3) one ray off the front wall, 4) one ray off the back wall, 5) one off the ceiling and 6) one off the floor. For the imaged antenna there are: 1) one ray that is directed straight to the receiving antenna, 2) one ray off each side wall, 3) one ray off the front wall, 4) one ray off the back wall, 5) one off the ceiling and 6) one ray off the floor. Figure 7 illustrates these rays.

To obtain our expression for site attenuation, the factor $E_{H,V}$ from (7) will be slightly rewritten here:

$$E_{H,V} = |\sum_{n=1}^{14}[\frac{e^{-jk_0r_n}}{r_n}F_T(\theta_n)\rho(\phi_n)F_R(\theta_n)]| \tag{9}$$

where $\rho(\phi_n)$ is the reflection coefficient of a ray incident at the wall at an angle ϕ_n, $F_R(\theta)$ is the antenna pattern of the receiving antenna, and $F_T(\theta)$ that of the transmitting antenna (here taken to be identical) and equal to:

$$F_R(\theta) = F_T(\theta) = \sin(\theta) \tag{10}$$

while θ_n is the angle that ray n makes to the vertical axis of the antennas (for our geometry, these angles are always the same for the transmitting and receiving antennas).

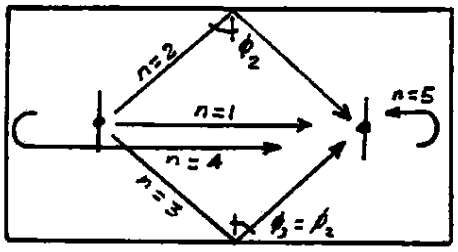

a) Top View

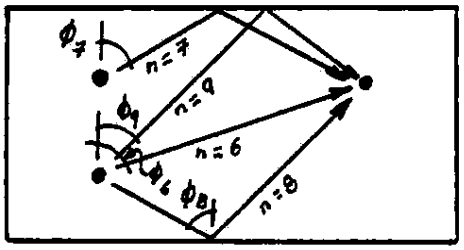

b) Side View I

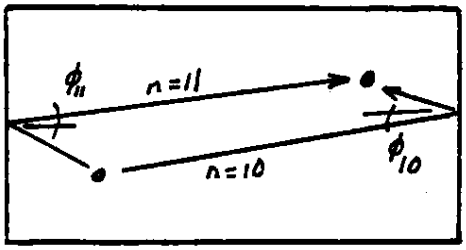

c) Side View II

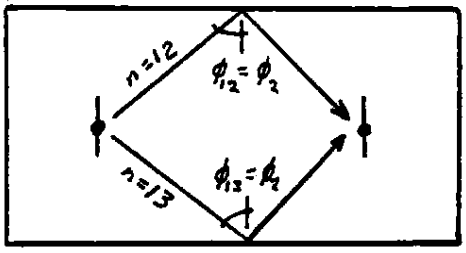

d) Top View of Image

Figure 7: Ray trajectories in the chamber.

To find E_H, the contributions from all the rays (see Figure 7) are all summed together. Therefore:

$$E_H = |(E_{TOP})_{total} + (E_{SIDE})_{total} + (E_{IMAGE})_{total}| \tag{11}$$

where:

$$\begin{aligned}(E_{TOP})_{total} &= \frac{e^{-jk_0r_2}}{r_2}\sin^2(\phi_2)\rho(\phi_2) + \frac{e^{-jk_0r_3}}{r_3}\sin^2(\phi_3)\rho(\phi_3) \\ &\quad + \frac{e^{-jk_0r_1}}{r_1} + \frac{e^{-jk_0r_4}}{r_4}\rho(0) + \frac{e^{-jk_0r_5}}{r_5}\rho(0)\end{aligned} \tag{12}$$

$$\begin{aligned}(E_{SIDE})_{total} &= \frac{e^{-jk_0r_7}}{r_7}\rho(\phi_7) - \frac{e^{-jk_0r_8}}{r_8}\rho(\phi_8) - \frac{e^{-jk_0r_9}}{r_9}\rho(\phi_9) \\ &\quad - \frac{e^{-jk_0r_6}}{r_6} - \frac{e^{-jk_0r_{10}}}{r_{10}}\rho(\phi_{10}) - \frac{e^{-jk_0r_{11}}}{r_{11}}\rho(\phi_{11})\end{aligned} \tag{13}$$

$$\tag{14}$$

and:

$$(E_{IMAGE})_{total} = -\frac{e^{-jk_0r_{12}}}{r_{12}}\rho(\phi_{12}) - \frac{e^{-jk_0r_{13}}}{r_{13}}\rho(\phi_{13}) \tag{15}$$

These three equations are substituted into equation (11) and then into equation (7) to obtain the site attenuation for the horizontal polarization.

The same procedure is followed to obtain the factor E_V for the vertical polarization. Equations (12), (13) and (15) become: for the top view,

$$\begin{aligned}(E_{TOP})_{total} &= \frac{e^{-jk_0r_2}}{r_2}\rho(\phi_2) + \frac{e^{-jk_0r_3}}{r_3}\rho(\phi_3) \\ &\quad + \frac{e^{-jk_0r_1}}{r_1} + \frac{e^{-jk_0r_4}}{r_4}\rho(0) + \frac{e^{-jk_0r_5}}{r_5}\rho(0)\end{aligned} \tag{16}$$

for the side views,

$$\begin{aligned}(E_{SIDE})_{total} &= \frac{e^{-jk_0r_7}}{r_7}\sin^2(\phi_7)\rho(\phi_7) + \frac{e^{-jk_0r_8}}{r_8}\sin^2(\phi_8)\rho(\phi_8) \\ &\quad + \frac{e^{-jk_0r_9}}{r_9}\sin^2(\phi_9)\rho(\phi_9) + \frac{e^{-jk_0r_6}}{r_6}\sin^2(\theta_6) \\ &\quad + \frac{e^{-jk_0r_{10}}}{r_{10}}\cos^2(\phi_{10})\rho(\phi_{10}) + \frac{e^{-jk_0r_{11}}}{r_{11}}\cos^2(\phi_{11})\rho(\phi_{11})\end{aligned} \tag{17}$$

and for the images,

$$(E_{IMAGE})_{total} = \frac{e^{-jk_0r_{12}}}{r_{12}}\sin^2(\theta_{12})\rho(\phi_{12}) + \frac{e^{-jk_0r_{13}}}{r_{13}}\sin^2(\theta_{13})\rho(\phi_{13}) \tag{18}$$

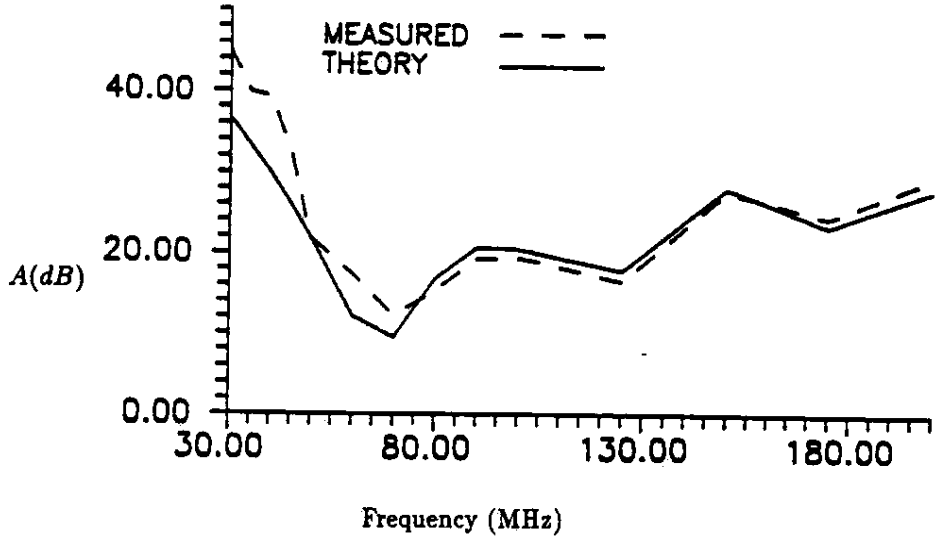

Figure 8: Comparison of the measured and theoretical site attenuation for the Boulder chamber (horizontal polarization).

5 Comparison with Measurements

To assess the accuracy of this model, we compare its predictions with measured data taken in semi-anechoic chambers at two IBM sites: Boulder, Colorado and Lexington, Kentucky. In both cases, identical biconical antennas were used for the transmitting and receiving antennas. Their antenna factors a_F over the frequency range of 30 to 200 MHz are given in Appendix A.

The dimensions of the Boulder chamber are shown in Figure 12 (see Appendix A). The reflection coefficient for the cones in this chamber was calculated theoretically as in [1], and is shown in Figure 13 (Appendix A). A computer program was written to calculate the necessary angles of incidence and the distance that each ray travels. These values were then substituted into the appropriate equation, depending upon the polarization used. The values were then compared to the actual measured site-attenuation which was also supplied by IBM. The horizontal polarization is shown in Figure 8 and the vertical polarization is shown in Figure 9.

The dimensions of the Lexington chamber are shown in Figure 14 (Appendix A). The theoretical reflection coefficient for the cones in the Lexington chamber is shown in Figure 15 (Appendix A). This figure represents the response curve of an array of six-foot cones with modified material properties [1]. Comparisons of the theoretical results with measurements are shown for the horizontal polarization in Figure 10 and for vertical polarization in Figure 11.

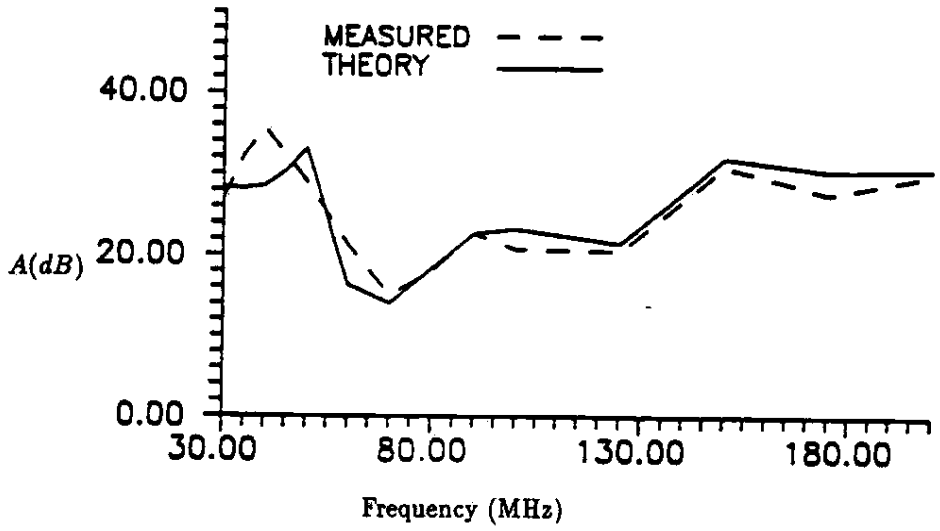

Figure 9: Comparison of the measured and theoretical site attenuation for the Boulder chamber (vertical polarization).

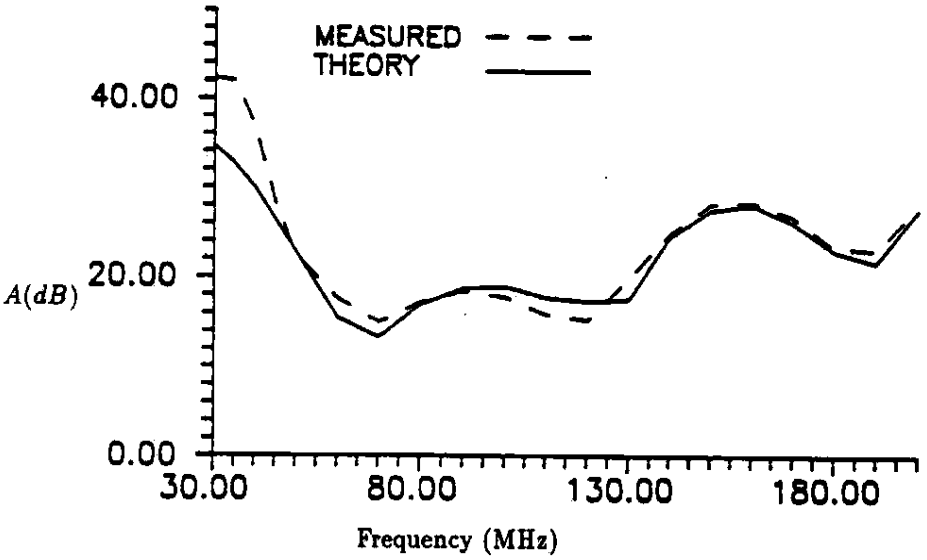

Figure 10: Comparison of the measured and theoretical site attenuation for the Lexington chamber (horizontal polarization).

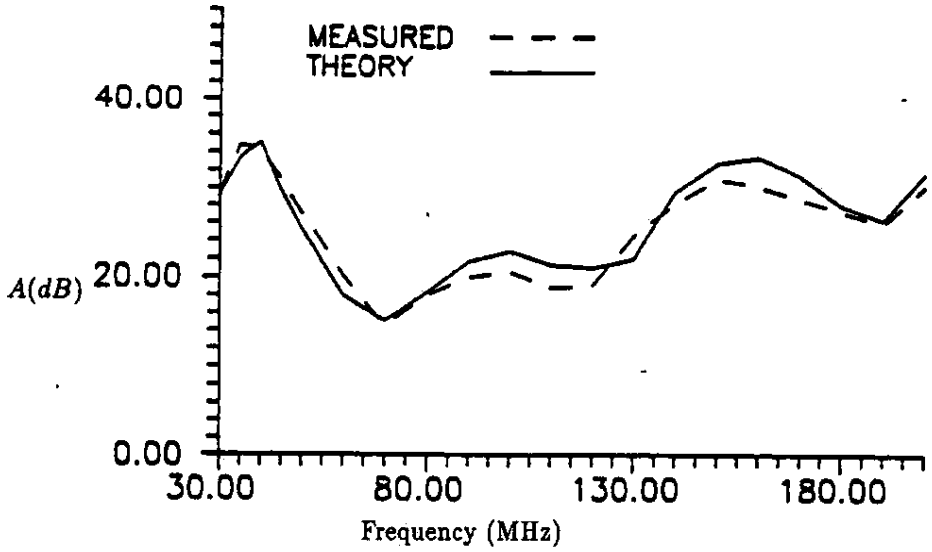

Figure 11: Comparison of the measured and theoretical site attenuation for the Lexington chamber (vertical polarization).

For the Boulder chamber (Figures 8 and 9), it is seen that the model differs at worst by about 6-7 dB for both polarizations. However, for the same chamber, by the time 70 MHz is attained the model has closed to within 1-1.5 dB of the experimental results.

Some of the poor correlation for the horizontal polarization may be due to the fact that the site attenuation used here neglects the mutual impedance between the two antennas (see [23]-[25], [27] for how this effect is included). In [28], German discusses the discrepancy between measured and calculated values of the site attenuation for both open-field sites and semi-anechoic chambers. For horizontal polarization, [28] indicates that neglecting this mutual impedance would cause an error of about 5 dB at 30 MHz.

Also in [28], a difference of approximately 1-2 dB between the calculated and measured values of the site attenuation for both polarizations in the frequency range 90-180 MHz is noted. This discrepancy may be associated with errors in the antenna factor used for both the transmitting and receiving antenna. This antenna factor error enters into our formulas and therefore may also contribute to the difference between our theory and measured site attenuation.

For the Lexington chamber, agreement is much better for vertical polarization as can be seen from Figure 11. The curves differ only about 1-1.5 dB over the whole frequency range, which is within what could be accounted for by the antenna factor error. For horizontal polarization we see that the curve correlates very well from 50 MHz up with discrepancies of only about 1-2 dB. Once

again, this may very well be due to the neglect of mutual impedance between the antennas.

6 Conclusion

Taking into account the assumptions that were made, it can be concluded that the model does a fairly good job of reproducing the experimental results. Let us take a more critical look at these assumptions. First, it was assumed that the walls were in the far field of the antennas. However, the dimension of the chamber placed the wall only about 3-5 meters from the antennas. Therefore, the far-field assumption is certainly strained in this comparison.

The most critical assumption that was made was that each ray attenuates enough after one bounce so that if the ray bounces off a second absorbing surface, the magnitude of the ray can be neglected. If one refers to Figure 13 (see Appendix A), where the reflection coefficient of one of the walls in the Boulder chamber is represented, it is observed that (from 30-60 MHz) at least 80 percent of the ray is reflected back. Therefore, if a ray makes two bounces, it will still contain enough energy so that neglecting its influence will cause considerable error.

For the Lexington chamber the one-bounce assumption is more valid, due to the response of the cones in that chamber. The response of the cones in the Lexington chamber is very similar to the curves in Figure 15. From this response it is shown that the reflection coefficient for low frequencies ranges from 50-70 percent which is much better than that for the Boulder cones, indicating that the one-bounce assumption is more accurate.

One other reason why the Lexington chamber model correlates to measured values better than the Boulder chamber is due to the material properties' values that were used in each analysis. For the Lexington chamber, the bulk parameters (ϵ and σ) that were used in the theoretical analysis were averages of those from four different material samples. As a result, material properties were used that were representative of the chamber parameters as a whole. For the Boulder chamber on the other hand, the bulk parameters were determined from only one sample and thus, may not have truly represented the material properties in the chamber.

Nevertheless, the comparisons made in the previous section indicate good agreement basically whenever the operating frequency is not near that of some room resonance. Presumably, most of the reflected rays are adding together in phase at such frequencies, and the assumption that further reflections from the absorbing walls are negligible is not warranted. Otherwise, these effects are subject to out-of-phase cancellations in a relatively random fashion, and a singly-reflected ray model will be accurate. It should be noted that comparisons of the ray method with more rigorous calculations have been made for acoustical anechoic chambers [9], [21], and have shown the same effect.

After analyzing the results of the chamber model and taking into account the assumptions and approximations, it is concluded that the chamber model is adequate, if the absorber has a sufficiently low reflection coefficient or if the operating frequency is not near a room resonance. Otherwise, a more sophisticated chamber model will have to be employed to achieve suitably accurate results.

References

[1] E. F. Kuester and C. L. Holloway, "Plane-wave reflection from inhomogeneous uniaxially anisotropic absorbing dielectric layers," *Sci. Rept. No. 97*, Electromagnetics Laboratory, Dept. of Electrical and Computer Engineering, Univerity of Colorado, Boulder, 1989.

[2] R.F. Kolar, "Fields in imperfect electromagnetic anechoic chambers," *RCA Review*, vol. 17, pp. 393-409, 1956.

[3] J. W. Wright and W. E. White, "Propagation in absorbent-material lined cavities," *Unclassified Proceedings of the Ninth Tri-Service Conference On Electromagnetic Compatibility*, 15-17 October, 1963, Chicago, pp. 656-667.

[4] R. R. Bowman, "Prevalent methods for evaluating anechoic chambers: Some basic limitations," in M.G. Arthur *et al.*, "High Frequency and Microwave Field Strength Precision Measurement Seminar," *National Bureau of Standards Report 9229*, 1966, Session III, Lecture 3.

[5] H. E. King, F. I. Shimabukuro and J. L. Wong, "Characteristics of a tapered anechoic chamber," *IEEE Trans. Ant. Prop.*, vol. 15, pp. 488-490, 1967.

[6] H. Hollmann, "Reflexionsarme Trichter- und Rechteckkammern für Antennenmessungen," *NTZ*, vol. 25, pp. 545-553, 1972.

[7] V. A. Torgovanov, "Anechoic chambers" [Russian], *Zarubezhnaya Radioelektronika*, no. 12, pp. 20-46, 1974.

[8] L. W. Pearson, J. R. Auton and Y. M. Lee, "Phenomenology of the intentional multipath reflections in a conically tapered anechoic chamber—A geometrical optics model," *Antenna Applications Symposium*, 20-22 September 1978, Urbana, Illinois.

[9] M. Gensane and F. Santon, "Prediction of sound fields in rooms of arbitrary shape: Validity of the image sources method," *J. Sound Vibration*, vol. 63, pp. 97-108, 1979.

[10] G. Benham, "A new approach to anechoic chambers," *Fourth Symposium on Electromagnetic Compatibility*, Zurich, 10-12 March 1981, pp. 395-400.

[11] M. Yu. Mitsmakher and V. A. Torgovanov, *Bezekhovye Kamery SVCh.* Moscow: Radio i Svyaz', 1982.

[12] M. C. Chandra Mouly and G. R. Reddy, "Performance evaluation of microwave anechoic chambers," *J. Inst. Eng. (India)*, vol. 63, part ET, pp. 84-86 (1982).

[13] L. Farber and H. R. Hofmann, "Correlation of theoretical and measured site attenuation in an absorber-lined chamber" *International Symposium on Electromagnetic Compatibility*, 23-25 August, 1983 Arlington, Va., pp.492-497.

[14] M. C. Chandra Mouly and V. Ranganadha Rao, "Effect of source antenna directivity on the performance of an anechoic chamber," *J. Inst. Eng. (India)*, vol. 64, part ET, pp. 60-62 (1984).

[15] M. C. Chandra Mouly and C. Raja Rao, "Rectangular and tapered microwave anechoic chambers: A comparative performance analysis," *J. Inst. Eng. (India)*, vol. 64, part ET, pp. 89-94 (1984).

[16] S. R. Mishra and T. J. F. Pavlasek. "Design of absorber-lined chambers for EMC measurements using a geometrical optics approach", *IEEE Trans. Electromag. Compat.*, vol. 26, pp. 111-119, 1984.

[17] J.D. Gavenda and J.H. Davis, "Electromagnetic wave propagation in a semi-anechoic chamber," *Sixth Symposium on Electromagnetic Compatibility*, Zurich, 5-7 March, 1985, pp. 65-68.

[18] M.C. Chandra, N. Vijaya Vani, N. Rukmini Devi, K. Sujata and V. Ranganadha Rao, "Design considerations for tapered microwave anechoic chambers," *J. Inst. Eng. (India)*, vol. 65, part ET, pp.60-64, 1985.

[19] M.C. Chandra Mouly, P.V. Sridevi, G. Mrudula and M. S. K. Reddy, "Design of cylindrical cap type structures for augmented performance of microwave anechoic chambers," *J. Inst. Eng. (India)*, vol. 68, part ET, pp. 59-62, 1988.

[20] M.C. Chandra, P.V. Sridevi, G. Mrudula and M.S.K. Reddy, "Design of wedge type structures for augmented performance of microwave anechoic chambers," *J. Inst. Eng. (India)*, vol. 69, part ET, pp. 1-4, 1988.

[21] G. Lemire and J. Nicolas, "Aerial propagation of spherical sound waves in bounded spaces," *J. Acoust. Soc. Amer.*, vol. 86, pp. 1845-1853, 1989.

[22] J. D. Gavenda, "Semi-anechoic chamber site attenuation calculations," *Seventh International Conference on Electromagnetic Compatibility*, York, UK, 28-31 August 1990, to appear.

[23] T. Kawana and S. Miyajima, "Theoretical investigations on site attenuation—Propagation characteristics inside the measuring site for the radio interference," *J. Radio Res. Lab. (Japan)*, vol. 25, no. 117/118, pp. 105-115, 1978.

[24] T. Kawana and S. Miyajima, "Theoretical investigations of site attenuation by means of mutual impedance between antennas—In the case of 3 meters distance between antennas," *J. Radio Res. Lab. (Japan)*, vol. 26, no. 120/121, pp. 135-145, 1979.

[25] T. Kawana, "Investigations of propagation characteristics of horizontally and vertically polarized waves in the 10 meter radiation measurement site," *J. Radio Res. Lab. (Japan)*, vol. 28, no. 125/126, pp. 73-85, 1981.

[26] A. A. Smith, Jr., R. F. German, and J. B. Pate, "Calculation of Site Attenuation From Antenna Factors," *IEEE Trans. Electromag. Compat.*, vol. 24, pp. 301-316 (1982).

[27] H.-D. Chuang and C.-F. Huang, "Near field effect on the evaluation of site attenuation," *J. Chinese Inst. Eng.*, vol. 12, pp. 331-339, 1989.

[28] R. F. German, "Comparison of Semi-Anechoic Chamber and Open-Field Site Attenuation Measurements," *IEEE International Symposium on Electromagnetic Compatibility*, pp. 260-265, 1982.

A Data For The IBM Chambers

This appendix contains the data for the antenna factor used in the calculation of site attenuation. Also shown in this appendix are the dimensions and absorber reflection coefficient data for both the Boulder and Lexington chambers. Both the antenna factors and the chamber dimensions were obtained from R. F. German at IBM, while the reflection coefficients were calculated by the methods of [1].

Table 1: Antenna factors for biconical antennas used in site attenuation measurements.

Frequency (MHz)	Antenna Factor dB/meter
30.0	13.0
35.0	13.2
40.0	13.0
45.0	12.2
50.0	11.0
60.0	7.4
70.0	5.9
80.0	8.8
90.0	10.9
100.0	11.5
110.0	11.1
125.0	11.7
140.0	15.5
150.0	17.3
160.0	17.7
170.0	16.6
180.0	14.8
190.0	13.8
200.0	16.3

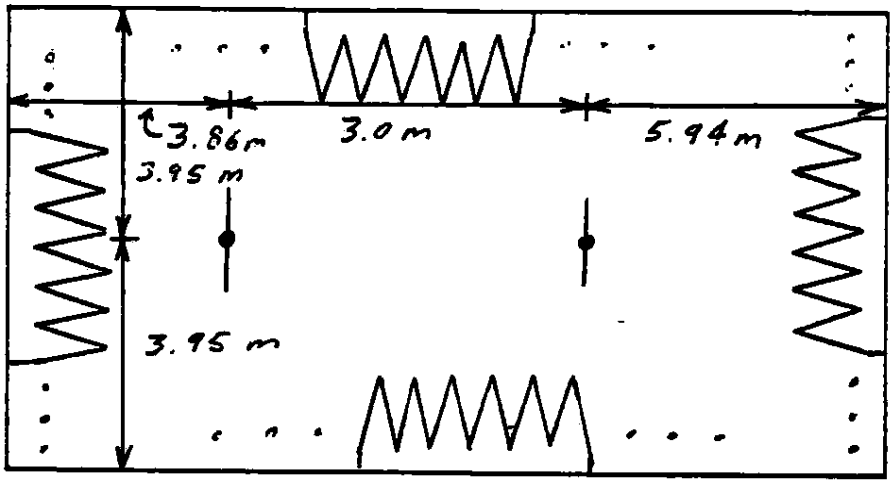

a) Top View

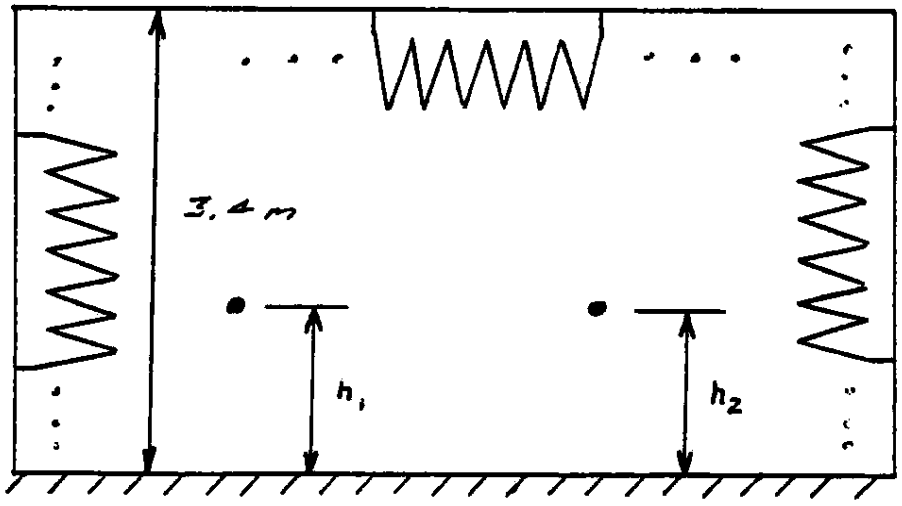

b) Side View

Figure 12: Dimensions for the Boulder chamber.

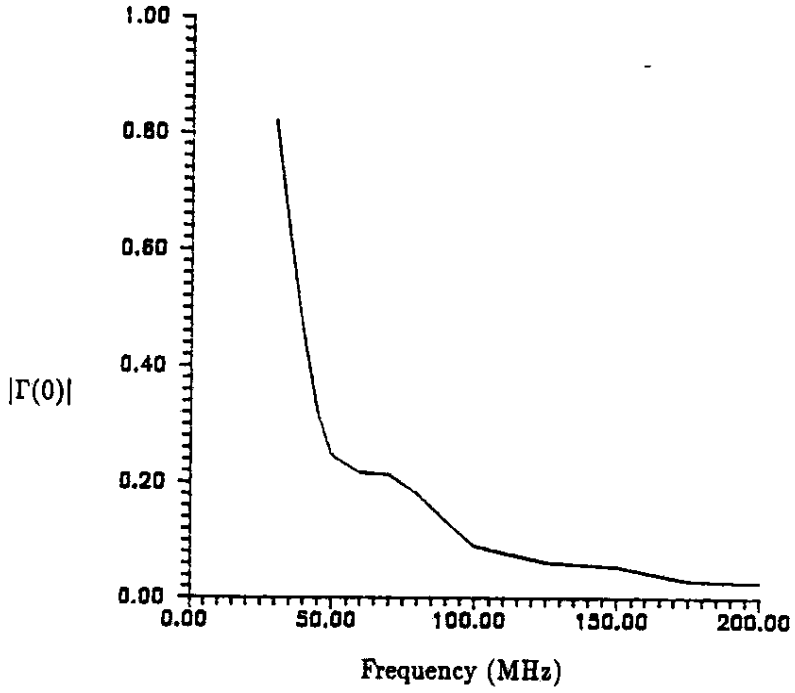

Figure 13: Reflection coefficient versus frequency for an array of typical absorbing cones in the Boulder chamber.

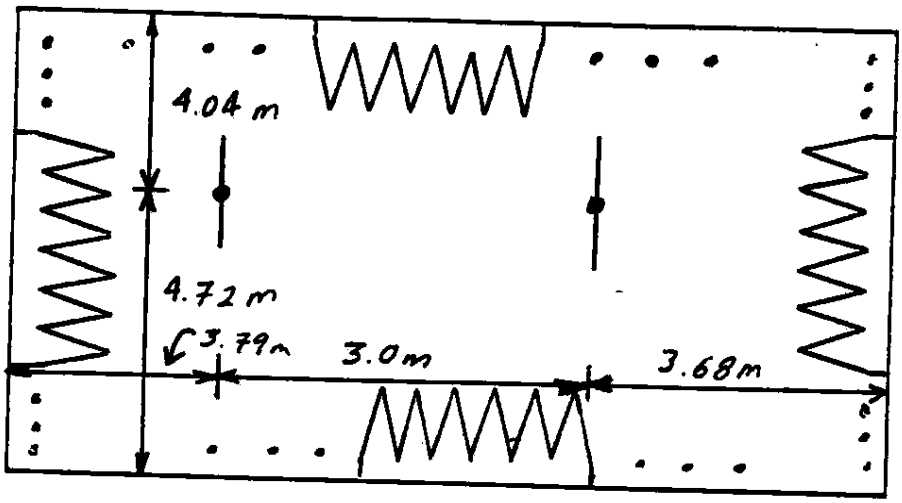

a) Top View

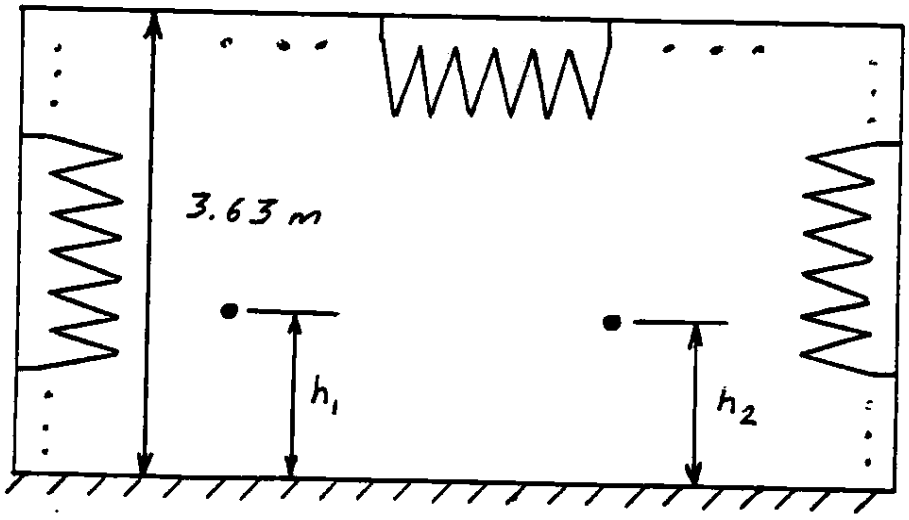

b) Side View

Figure 14: Dimensions for the Lexington chamber.

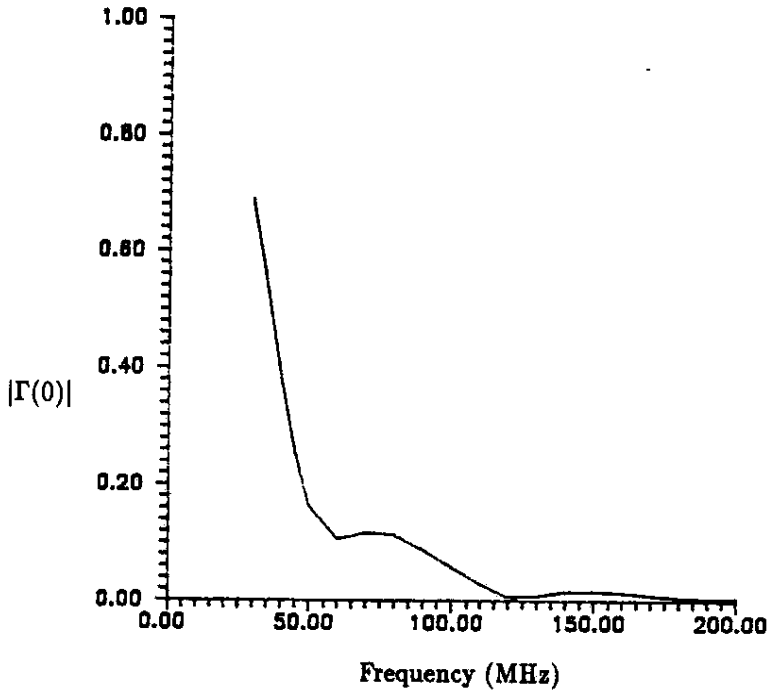

Figure 15: Reflection coefficient versus frequency for an array of typical absorbing cones in the Lexington chamber.